Supplement of Atmos. Chem. Phys., 25, 14315–14331, 2025
https://doi.org/10.5194/acp-25-14315-2025-supplement


Atmospheric Chemistry and Physics
Open Access
EGU

*Supplement of*

# Reaction between linear perfluoroaldehydes and hydroperoxy radical in the atmosphere: reaction mechanisms, reaction kinetics modelling, and atmospheric implications

**Zegang Dong et al.**

*Correspondence to:* Bo Long (wwwltcommon@sina.com)

**TABLE OF CONTENTS**

## METHODS

### Computation details of multi-structural method for torsional anharmonicity

### (a)Theoretical background

The complete conformational-rotational-vibrational partition functions involving reactant and transition state have been all calculated by using MS-T method (multi-structural method for torsional anharmonicity)(Zheng and Truhlar, 2013) and executed through MSTor program package.(Chen et al., 2023) In general, the conformational-rotational-vibrational partition function is calculated as,

$$Q_{con-rovib}^{MS-T,X} = \sum_{j=1}^{J} Q_{rot,j}\, exp(-\beta U_j)\, Q_j^{HO}\, Z_j \prod_{t=1}^{t} f_{j,\tau} \qquad (1)$$

where “con” and “rovib” denote conformation and rotation-vibration, respectively, $J$ is the number of distinguishable conformational structures ($j$ = 1, 2, ⋯, $J$). β = 1/$k_b$T and $X$ labels reactants, products or transition states. $Q_{rot,j}$, $U_j$ and $Q_j^{HO}$ represent the classical rotational partition of structure $j$, energy gap relative to the global minimum energy structure, and the normal-mode harmonic oscillator vibration partition function of the $J^{th}$ structure, respectively. $Z_j$ is a factor to ensure that the MS-T scheme reaches the correct high-Temperature limit (within the parameter range of the model), and $f_{j,\tau}$ is an internal coordinate torsional nonharmonic function that adjusts the harmonic partition function of structure $j$ to account for torsional motion $\tau$.

When equation (1) is used for a single-structure (SS) rotation-vibrational partition function of the conformer $j$ (generally, the global minima structure ($j$ = 1)), and if $Z_j$ and $f_{j,\tau}$ were set to 1, the partition function $Q_{con-rovib}^{MS-T,X}$ reduces to the multi-structural local-harmonic (MS-LH) partition function. Thus, we

can rewrite it as

$$Q_{rovib,j}^{SS-HO} = Q_{rot,j}\, exp(-\beta U_j)\, Q_{vib,j}^{HO} \quad (2)$$

Subsequently, the multistructural torsional anharmonicity factor $F^{MS-T,X}$ will be defined for reactants and transition states by using equation (1) and (2) as shown below

$$F^{MS-T,X} = Q_{con-rovib}^{MS-T,X} / Q_{rovib,1}^{SS-HO} \quad (3)$$

also, the corresponding multi-structural torsional anharmonicity factor for the reaction

$$F^{MS-T,X} = Q_{sp}^{MS-T} / Q_R^{MS-T} \quad (4)$$

The bimolecular rate constant was calculated as

$$k^{MS-T} = \kappa\sigma \frac{k_B T}{h} \frac{Q_{elec}^{\neq} Q_{con-rovib}^{MS-T,\neq}}{N_a Q_{elec}^{R} Q_{con-rovib}^{MS-T,R}} exp(-\beta V^{\neq}) \quad (5)$$

where $k_b$ is Boltzmann's constant, T is the temperature, N is Avogadro's number, $h$ is Planck's constant, and β is $1/k_b$T. $V^{\neq}$ denotes the classic reaction energy barrier exclude ZPE correction. $Q_{elec}$ represent electronic partition function, while κ and σ denote Eckart tunneling coefficient and the reaction symmetry number, respectively.

**(b) Calculated details**

(1) Conformational Search: Use **ConfGen.exe** to generate initial structures by rotating specified bonds

(2) Geometry Optimization & Frequency Calculation: Optimize structures using Gaussian and remove duplicates (e.g., mirrored/rotationally equivalent structures). Run frequency calculations to obtain Hessians and energies.

(3) Distinct Structure Identification: Use **mvinput.exe** to exclude mirror images and rotationally redundant structures. Generate *mvorm.inp* for Voronoi tessellation

(4) Torsional Periodicity ($M_{j,\tau}$): Compute $M_{j,\tau}$ values using **mcvorm.exe** (Monte Carlo) or vorm.exe (Voronoi tessellation).

(5) Input File Generation: Combine Gaussian .fchk files into *all.fchk*. Use **msinput.exe** to generate *mstor.inp* and *hess.dat*, adding uncoupled torsions.

(6) Execution: Run mstor.exe with the MS-T(CD) method to calculate partition functions and thermodynamic properties.

**(c) Input files for the ConfGen.exe executable**

13 2

| | | | |
|---|---|---|---|
| C | 1.01911500 | -0.47626600 | 0.05443400 |
| C | 2.35234900 | 0.19807600 | 0.44862800 |
| H | 2.51946100 | 0.29297300 | 1.53563000 |
| C | -0.15660500 | 0.51749400 | 0.11794900 |
| O | 3.12769000 | 0.56284200 | -0.38553200 |
| F | 0.04052700 | 1.46045400 | -0.81804700 |
| F | -0.13406100 | 1.10278400 | 1.33631400 |
| F | 1.10175100 | -0.98403000 | -1.18192700 |
| F | 0.78274500 | -1.47995300 | 0.93436300 |
| C | -1.56560300 | -0.07991200 | -0.09014200 |
| F | -2.45510800 | 0.91017100 | -0.11075900 |
| F | -1.62361100 | -0.73826800 | -1.24442900 |
| F | -1.87185600 | -0.91027500 | 0.90264400 |

#torsion 1 definition
2 1
3
5 2 3
3
0.0 120.0 -120.0
#torsion 2 definition
1 4
6
1 8 9 2 3 5
3
0.0 120.0 -120.0
%nprocshared=12
%mem=80GB
# M062x/gen opt=calcfc int=grid=99974 scf=conver=11
0 1
@/home/zgdong/mg3s.gbs
Extbasis

**Computation details of torsional anharmonicity factor for the forward reaction of $HO_2$ with XCHO (X=H, $C_2F_5$, and $C_3F_7$)**

The multi-structural torsional anharmonicity factor of the forward reaction is defined as

$$F_{\mathrm{fwd}}^{\mathrm{MS-T}} = \frac{F^{\mathrm{MS-T}}(\mathrm{TS})}{F^{\mathrm{MS-T}}(\mathrm{R})} = \frac{Q^{\ddagger-\mathrm{MS-T}}/Q^{\ddagger-\mathrm{SS-HO}}}{Q^{\mathrm{R-MS-T}}/Q^{\mathrm{R-SS-HO}}} \qquad \text{(S1)}$$

Where:

$Q^{\ddagger-\mathrm{MS-T}}$ is the multi-structural partition functions for the saddle points,

$Q^{\mathrm{R-MS-T}}$ is the multi-structural partition functions for the reactants,

$Q^{\ddagger-\mathrm{SS}-\mathrm{HO}}$ is the single-structural harmonic-oscillator rovibrational partition functions for the lowest energy saddle point,

$Q^{\mathrm{R}-\mathrm{SS}-\mathrm{HO}}$ is the single-structural harmonic-oscillator rovibrational partition functions for the lowest energy reactant.

**Computational details of pressure-dependent rate constants**

For SS-QRRK calculations, $F_E$ is determined through the numerically integrated Whitten-Rabinovitch approximation. We considered the same activation mechanisms as equation (2) in previous studies.(Long et al., 2022) In our recent review, the SS-QRRK approach for the activation mechanism under consideration is shown in Equation 193.(Bao and Truhlar, 2017) Collision efficiency is computed utilizing the exponential-down model with the energy transfer parameter <ΔE > down set at 300 $cm^{-1}$. Additionally, Lennard-Jones (L-J) parameters for the collision rates calculations are as follow:

| Molecule | ε (in K) | σ (in Å) | Reference |
|---|---|---|---|
| $N_2$ bath gas | 82 | 3.74 | (Kuwata et al., 2010) |
| He bath gas | 10 | 2.55 | (Kuwata et al., 2010) |
| Air bath gas | 86.2 | 3.688 | - |
| $HO_2$ | 289.3 | 4.2 | (Troe, 1977) |
| $C_3H_7O_3$[a] | 508.25 | 3.62 | (Xi et al., 2021) |

[a]The line of $C_3H_7O_3$ denotes the Lennard-Jones (L-J) parameters of product

**Computational details of metadynamics-biased ab initio molecular dynamics (AIMD)**

In the AIMD simulations, the air–water nanodroplet interface model constructed here included $C_2F_5CHO$ and water nanodroplets, each composed of 21 water molecules. To avoid interactions between periodic replicas of adjacent water nanodroplets, the simulation box was dimensioned as 20 Å× 20 Å× 20 Å. The Becke–Lee–Yang–Parr (BLYP) functional was combined with Grimme's dispersion correction (BLYP-D3) to properly account for weak dispersion forces. (Becke, 1988; Grimme, 2004, 2006; Lee et al., 1988) Valence electrons were described using a double-ζ Gaussian basis set (DZVP) with an auxiliary basis set, while core electrons were treated via Goedecker-Teter-Hutter (GTH) norm-conserving pseudopotentials. (Goedecker and Teter, 1996; Hartwigsen et al., 1998; VandeVondele and Hutter, 2007) The cutoff energies for plane-wave and Gaussian basis sets were set to 280 and 40 Rydberg, respectively.

All simulations were conducted under the NVT ensemble (constant volume and temperature at 300 K), with temperature regulation achieved using the Nose – Hoover chain algorithm. (Hoover and Alder, 1967; Nosé, 1984) A fixed time step of 0.5 fs was employed.

Metadynamics serves as a powerful enhanced sampling technique, accelerating conformational sampling by introducing a history-dependent bias potential that depends on selected collective variables (CVs). (Laio and Parrinello, 2002) For exploring the hydrolysis mechanisms of $C_2F_5CHO$, we utilized a advanced of metadynamics known as stepwise multi-subphase space metadynamics, (Fang et al., 2022) alongside reconstructing the corresponding free energy profiles at the air – water nanodroplet interface. Within the CP2K software package, (Kühne et al., 2020) the metadynamics setup is defined by three key parameters for Gaussian hills: a height of 0.2 kcal·mol$^{-1}$, a width of 0.1 Å, and an update interval of 30 fs. Quadratic wall potentials were applied to confine the sampling region. Additionally, the kinetic evaluation of the air-water interface is assessed according to conventional transition state theory.

**RESULT**

**Table S1**. Specific reaction scale factors calculated by using the MPW1K/6-311 + G(2df,2p) method.

| | $C_2F_5CHO$ | $C_3F_7CHO$ | $HO_2$ | RC1 | TS1 | P1 | RC2 | TS2 | P2 |
|---|---|---|---|---|---|---|---|---|---|
| ZPE(Harm) | 29.864 | 38.071 | 9.448 | 41.2 | 40.292 | 43.165 | 49.259 | 48.349 | 51.268 |
| ZPE(Anh) | 29.659 | 37.816 | 9.308 | 40.727 | 39.199 | 42.701 | 48.696 | 47.086 | 50.809 |
| [a]$\lambda^{Ahn}$ | 0.993 | 0.993 | 0.985 | 0.989 | 0.973 | 0.989 | 0.989 | 0.974 | 0.991 |
| [b]$\lambda^{ZPE}$ | 0.975 | 0.975 | 0.967 | 0.971 | 0.955 | 0.971 | 0.971 | 0.956 | 0.973 |

[a]$\lambda^{Ahn}$= ZPE(Anh)/ZPE(Harm)

[b]$\lambda^{ZPE}=\lambda^{Ahn}*\lambda^{H}$, $\lambda^{H}$ is 0.982 for the M06-2X/MG3S method.

**Table S2**. The enthalpy of activation at 0 K for $HO_2$ reaction with XCHO (X = $C_2F_5$ and $C_3F_7$) (in kcal/mol).

| Methods | $\Delta V^a$ | | | | | |
|---|---|---|---|---|---|---|
| | RC1 | RC2 | TS1 | TS2 | P1 | P2 |
| CCSD(T)-F12a/cc-pVTZ-F12//M06-2X/MG3S[a] | -5.4 | -5.5 | **-2.7** | **-2.7** | -14.8 | -14.7 |
| CCSD(T)-F12a/cc-pVTZ-F12//M06-2X/MG3S[b] | -5.5 | -5.5 | **-3.5** | **-3.6** | -14.8 | -14.7 |
| Effect of scale factor | 0.1 | 0.0 | **0.8** | **0.9** | 0.0 | 0.0 |

[a]The enthalpy of activation at 0 K calculated with harmonic zero-point vibration energy using a standard scale factor.

[b]The enthalpy of activation at 0 K calculated with harmonic zero-point vibration energy using the reaction-specific scale factors obtained by using HDCVPT with the electronic structure carried out by MPW1K/6-311+G(2df,2p).

**Table S3**. Zero-point vibrational energies relative to reactants and their mean unsigned deviations from best estimates.

| Methods | Level | $\Delta V^a$ | | | | | | |
|---|---|---|---|---|---|---|---|---|
| | | RC1 | RC2 | TS1 | TS2 | P1 | P2 | MUE[b] |
| CCSD(T)-F12a/cc-pVTZ-F12//M06-2X/MG3S[c] | High Level (HL) | -5.4 | -5.5 | -2.7 | -2.7 | -14.8 | -14.7 | 0.0 |
| M11-L/maug-cc-pVTZ[c] | Low Level (LL) | -5.4 | -5.4 | -2.8 | -2.7 | -12.7 | -12.6 | 0.7 |

[a]Energy difference of pre-reaction complexes, transition-states, and products relative to its reactants, respectively.

[b]Mean unsigned error averaged over the six previous columns

[c]The scale factors for vibrational frequency calculations using the M06-2X/MG3S and M11-L/maug-cc-pVTZ methods are 0.970 and 0.985, respectively.

**Table S4**. Fitting parameters for HPL rate constants

| Reaction | lnA | T0 | n | E |
|---|---|---|---|---|
| $C_2F_5CHO+HO_2$ | -36.13 | 20.07 | 1.27 | -3.51 |
| $C_3F_7CHO+HO_2$ | -36.39 | 34.23 | 1.24 | -3.28 |

**Table S5**. The conventional transition state theory (TST) rate constants ($cm^3 \cdot molecules^{-1} \cdot s^{-1}$) without a transmission coefficient for $HO_2$ + XCHO (X= $C_2F_5$ and $C_3F_7$) reactions at the temperature range 190-350 K.

| T/K | $k_1^{SS-HO}$ [a] | $k_1^{SS-HO'}$ [b] | $k_2^{SS-HO}$ [a] | $k_2^{SS-HO'}$ [b] | $f_1$ [c] | $f_2$ [c] |
|---|---|---|---|---|---|---|
| 190 K | 8.53E-12 | 1.17E-12 | 7.70E-12 | 7.58E-13 | 7.28E+00 | 1.02E+01 |
| 200 K | 5.23E-12 | 7.85E-13 | 4.68E-12 | 5.10E-13 | 6.66E+00 | 9.17E+00 |
| 210 K | 3.36E-12 | 5.47E-13 | 2.98E-12 | 3.56E-13 | 6.14E+00 | 8.36E+00 |
| 220 K | 2.25E-12 | 3.94E-13 | 1.98E-12 | 2.57E-13 | 5.71E+00 | 7.69E+00 |
| 230 K | 1.56E-12 | 2.92E-13 | 1.36E-12 | 1.91E-13 | 5.35E+00 | 7.13E+00 |
| 240 K | 1.12E-12 | 2.22E-13 | 9.71E-13 | 1.46E-13 | 5.03E+00 | 6.65E+00 |
| 250 K | 8.24E-13 | 1.73E-13 | 7.12E-13 | 1.14E-13 | 4.76E+00 | 6.25E+00 |
| 260 K | 6.23E-13 | 1.37E-13 | 5.35E-13 | 9.07E-14 | 4.53E+00 | 5.90E+00 |
| 270 K | 4.81E-13 | 1.11E-13 | 4.11E-13 | 7.35E-14 | 4.32E+00 | 5.59E+00 |
| 280 K | 3.78E-13 | 9.14E-14 | 3.22E-13 | 6.06E-14 | 4.14E+00 | 5.32E+00 |
| 290 K | 3.03E-13 | 7.62E-14 | 2.57E-13 | 5.06E-14 | 3.98E+00 | 5.09E+00 |
| 298 K | 2.57E-13 | 6.65E-14 | 2.18E-13 | 4.43E-14 | 3.86E+00 | 4.92E+00 |
| 300 K | 2.47E-13 | 6.44E-14 | 2.09E-13 | 4.29E-14 | 3.84E+00 | 4.88E+00 |
| 310 K | 2.04E-13 | 5.51E-14 | 1.72E-13 | 3.67E-14 | 3.71E+00 | 4.69E+00 |
| 320 K | 1.71E-13 | 4.76E-14 | 1.44E-13 | 3.18E-14 | 3.59E+00 | 4.52E+00 |
| 330 K | 1.45E-13 | 4.16E-14 | 1.22E-13 | 2.78E-14 | 3.49E+00 | 4.37E+00 |
| 340 K | 1.24E-13 | 3.67E-14 | 1.04E-13 | 2.46E-14 | 3.39E+00 | 4.24E+00 |
| 350 K | 1.08E-13 | 3.26E-14 | 9.00E-14 | 2.19E-14 | 3.30E+00 | 4.11E+00 |

[a] $k_1^{SS-HO}$ and $k_2^{SS-HO}$ are the conventional transition state theory rate constants calculated using the Single-Structure Harmonic-Oscillator (SS-HO) method with the specific-reaction scale factors.

[b] $k_1^{SS-HO'}$ and $k_2^{SS-HO'}$ are the conventional transition state theory rate constants calculated using the Single-Structure Harmonic-Oscillator (SS-HO) method with the standard vibrational-frequency scale factors.

[c] $f_1$ *and* $f_2$ are equal to $k_1^{SS-HO}/k_1^{SS-HO'}$ and $k_2^{SS-HO}/k_2^{SS-HO'}$, and represent the ratios for the reactions of $C_2F_5CHO$ + $HO_2$ and $C_3F_7CHO$ + $HO_2$, respectively.

**Table S6**. Multi-structural torsional anharmonicity factors of the forward reaction of $HO_2$ with XCHO (X=$C_2H_5$, and $C_3F_7$) as functions of temperature.

| T/K | $F_{C2F5CHO}^{MS-T}$ [a] | $F_{C3F7CHO}^{MS-T}$ [b] | $F_{TS1}^{MS-Ta}$ | $F_{TS2}^{MS-Tb}$ | $F_1^{MS-Tc}$ | $F_2^{MS-Tc}$ |
|---|---|---|---|---|---|---|
| 190 K | 3.978 | 6.714 | 2.249 | 3.025 | 5.65E-01 | 4.51E-01 |
| 200 K | 4.029 | 6.838 | 2.287 | 3.112 | 5.68E-01 | 4.55E-01 |
| 210 K | 4.076 | 6.954 | 2.326 | 3.196 | 5.71E-01 | 4.60E-01 |
| 220 K | 4.118 | 7.061 | 2.365 | 3.278 | 5.74E-01 | 4.64E-01 |
| 230 K | 4.157 | 7.161 | 2.406 | 3.359 | 5.79E-01 | 4.69E-01 |
| 240 K | 4.192 | 7.255 | 2.446 | 3.438 | 5.83E-01 | 4.74E-01 |
| 250 K | 4.224 | 7.342 | 2.487 | 3.514 | 5.89E-01 | 4.79E-01 |
| 260 K | 4.254 | 7.423 | 2.529 | 3.589 | 5.94E-01 | 4.83E-01 |
| 270 K | 4.281 | 7.498 | 2.571 | 3.663 | 6.01E-01 | 4.89E-01 |
| 280 K | 4.305 | 7.569 | 2.612 | 3.734 | 6.07E-01 | 4.93E-01 |
| 290 K | 4.327 | 7.634 | 2.654 | 3.804 | 6.13E-01 | 4.98E-01 |
| 298 K | 4.344 | 7.683 | 2.688 | 3.859 | 6.19E-01 | 5.02E-01 |
| 300 K | 4.347 | 7.695 | 2.696 | 3.873 | 6.20E-01 | 5.03E-01 |
| 310 K | 4.366 | 7.751 | 2.737 | 3.939 | 6.27E-01 | 5.08E-01 |
| 320 K | 4.383 | 7.804 | 2.779 | 4.005 | 6.34E-01 | 5.13E-01 |
| 330 K | 4.398 | 7.852 | 2.82 | 4.069 | 6.41E-01 | 5.18E-01 |
| 340 K | 4.411 | 7.897 | 2.861 | 4.131 | 6.49E-01 | 5.23E-01 |
| 350 K | 4.424 | 7.938 | 2.901 | 4.193 | 6.56E-01 | 5.28E-01 |

[a] Multi-structural torsional anharmonicity factors for the $C_2F_5CHO$ and correspond transition states.

[b] Multi-structural torsional anharmonicity factors for the $C_3F_7CHO$ and correspond transition states.

[c] $F_1^{MS-T}$ $and$ $F_2^{MS-T}$ are the torsional anharmonicity factors of the forward reaction of $HO_2$ with XCHO (X=$C_2H_5$, and $C_3F_7$), and are equal to $F_{TS1}^{MS-T}/F_{C2F5CHO}^{MS-T}$ and $F_{TS1}^{MS-T}/F_{C3F7CHO}^{MS-T}$.

**Table S7**. HPL transmission coefficients for $HO_2$ + XCHO (X= $C_2F_5$ ("label 1")) and $C_3F_7$ ("label 2")) reactions.

| T/K | $k_{TST}^{HL-1a}$ | $\Gamma_{CVT}^{LL-1b}$ | $k_{SCT}^{LL-1c}$ | $k_{TST}^{HL-2a}$ | $\Gamma_{CVT}^{LL-2b}$ | $k_{SCT}^{LL-2c}$ |
|---|---|---|---|---|---|---|
| 190 K | 4.82E-12 | 4.43E-01 | 1.57E+00 | 3.47E-12 | 4.26E-01 | 1.53E+00 |
| 200 K | 2.97E-12 | 4.66E-01 | 1.49E+00 | 2.13E-12 | 4.47E-01 | 1.46E+00 |
| 210 K | 1.92E-12 | 4.87E-01 | 1.43E+00 | 1.37E-12 | 4.68E-01 | 1.41E+00 |
| 220 K | 1.29E-12 | 5.08E-01 | 1.38E+00 | 9.19E-13 | 4.88E-01 | 1.36E+00 |
| 230 K | 9.04E-13 | 5.27E-01 | 1.34E+00 | 6.40E-13 | 5.07E-01 | 1.32E+00 |
| 240 K | 6.53E-13 | 5.46E-01 | 1.30E+00 | 4.60E-13 | 5.25E-01 | 1.29E+00 |
| 250 K | 4.85E-13 | 5.64E-01 | 1.27E+00 | 3.41E-13 | 5.42E-01 | 1.26E+00 |
| 260 K | 3.70E-13 | 5.81E-01 | 1.25E+00 | 2.59E-13 | 5.59E-01 | 1.24E+00 |
| 270 K | 2.89E-13 | 5.97E-01 | 1.23E+00 | 2.01E-13 | 5.75E-01 | 1.22E+00 |
| 280 K | 2.30E-13 | 6.13E-01 | 1.21E+00 | 1.59E-13 | 5.90E-01 | 1.20E+00 |
| 290 K | 1.86E-13 | 6.25E-01 | 1.19E+00 | 1.28E-13 | 6.05E-01 | 1.19E+00 |
| 298 K | 1.59E-13 | 6.34E-01 | 1.18E+00 | 1.09E-13 | 6.16E-01 | 1.18E+00 |
| 300 K | 1.53E-13 | 6.36E-01 | 1.18E+00 | 1.05E-13 | 6.19E-01 | 1.17E+00 |
| 310 K | 1.28E-13 | 6.47E-01 | 1.16E+00 | 8.76E-14 | 6.32E-01 | 1.16E+00 |
| 320 K | 1.08E-13 | 6.56E-01 | 1.15E+00 | 7.39E-14 | 6.45E-01 | 1.15E+00 |
| 330 K | 9.30E-14 | 6.65E-01 | 1.14E+00 | 6.31E-14 | 6.57E-01 | 1.14E+00 |
| 340 K | 8.06E-14 | 6.74E-01 | 1.13E+00 | 5.45E-14 | 6.66E-01 | 1.13E+00 |
| 350 K | 7.06E-14 | 6.82E-01 | 1.13E+00 | 4.75E-14 | 6.74E-01 | 1.12E+00 |

[a] $k_{TST}^{HL-1}$ ( $k_{TST}^{HL} = k_1^{SS-HO} * F_1^{MS-T}$ ) and $k_{TST}^{HL-2}$ ( $k_{TST}^{HL} = k_2^{SS-HO} * F_2^{MS-T}$ ) are the rate constants including torsional anharmonicity factor and without a transmission coefficient, which are calculated by the reaction-specific scale factor.

[b] $\Gamma_{CVT}^{LL-1}$ and $\Gamma_{CVT}^{LL-2}$ are the low-level recrossing transmission coefficients, which equal $k_{CVT}^{LL-1}/k_{TST}^{LL-1}$ and $k_{CVT}^{LL-2}/k_{TST}^{LL-2}$calculated by the scale factor from the standard method.

[c] $k_{SCT}^{LL-1}$ *and* $k_{SCT}^{LL-2}$ are the low-level tunneling transmission coefficients calculated by the small-curvature tunneling approximation with the scale factor from the standard method.

**Table S8**. The pressure-dependent rate constants ($cm^3$ $molecule^{-1}$ $s^{-1}$) of $HO_2$ + $C_2F_5CHO$ reaction calculated by the SS-QRRK method.

| $p$ (bar) | 350 $K$ | 330 K | 310 K | 298 K | 290 $K$ |
|---|---|---|---|---|---|
| 0.0316 | 3.91E-14 | 5.74E-14 | 8.46E-14 | 1.08E-13 | 1.29E-13 |
| 0.0667 | 4.42E-14 | 6.24E-14 | 8.95E-14 | 1.13E-13 | 1.33E-13 |
| 0.1 | 4.64E-14 | 6.45E-14 | 9.14E-14 | 1.15E-13 | 1.35E-13 |
| 0.178 | 4.90E-14 | 6.67E-14 | 9.33E-14 | 1.16E-13 | 1.37E-13 |
| 0.316 | 5.08E-14 | 6.82E-14 | 9.46E-14 | 1.17E-13 | 1.38E-13 |
| 0.562 | 5.21E-14 | 6.92E-14 | 9.53E-14 | 1.18E-13 | 1.38E-13 |
| 1 | 5.29E-14 | 6.98E-14 | 9.58E-14 | 1.18E-13 | 1.39E-13 |
| 1.78 | 5.34E-14 | 7.02E-14 | 9.60E-14 | 1.19E-13 | 1.39E-13 |
| 3.16 | 5.38E-14 | 7.04E-14 | 9.62E-14 | 1.19E-13 | 1.39E-13 |
| 5.62 | 5.39E-14 | 7.05E-14 | 9.63E-14 | 1.19E-13 | 1.39E-13 |
| 10 | 5.41E-14 | 7.06E-14 | 9.63E-14 | 1.19E-13 | 1.39E-13 |
| 31.6 | 5.42E-14 | 7.07E-14 | 9.64E-14 | 1.19E-13 | 1.39E-13 |
| 100 | 5.42E-14 | 7.07E-14 | 9.64E-14 | 1.19E-13 | 1.39E-13 |
| 1000 | 5.42E-14 | 7.07E-14 | 9.64E-14 | 1.19E-13 | 1.39E-13 |
| $p$ (bar) | 270$K$ | 250 $K$ | 230 K | 210 K | 190 K |
| 0.0316 | 2.02E-13 | 3.41E-13 | 6.30E-13 | 1.32E-12 | 3.34E-12 |
| 0.0667 | 2.06E-13 | 3.44E-13 | 6.33E-13 | 1.33E-12 | 3.35E-12 |
| 0.1 | 2.08E-13 | 3.45E-13 | 6.35E-13 | 1.33E-12 | 3.35E-12 |
| 0.178 | 2.09E-13 | 3.47E-13 | 6.36E-13 | 1.33E-12 | 3.35E-12 |
| 0.316 | 2.10E-13 | 3.47E-13 | 6.36E-13 | 1.33E-12 | 3.35E-12 |
| 0.562 | 2.10E-13 | 3.48E-13 | 6.37E-13 | 1.33E-12 | 3.35E-12 |
| 1 | 2.11E-13 | 3.48E-13 | 6.37E-13 | 1.33E-12 | 3.35E-12 |
| 1.78 | 2.11E-13 | 3.48E-13 | 6.37E-13 | 1.33E-12 | 3.35E-12 |
| 3.16 | 2.11E-13 | 3.48E-13 | 6.37E-13 | 1.33E-12 | 3.35E-12 |
| 5.62 | 2.11E-13 | 3.48E-13 | 6.37E-13 | 1.33E-12 | 3.35E-12 |
| 10 | 2.11E-13 | 3.48E-13 | 6.37E-13 | 1.33E-12 | 3.35E-12 |
| 31.6 | 2.11E-13 | 3.48E-13 | 6.37E-13 | 1.33E-12 | 3.35E-12 |
| 100 | 2.11E-13 | 3.48E-13 | 6.37E-13 | 1.33E-12 | 3.35E-12 |
| 1000 | 2.11E-13 | 3.48E-13 | 6.37E-13 | 1.33E-12 | 3.35E-12 |

**Table S9**. The pressure-dependent rate constants ($cm^3$ $molecule^{-1}$ $s^{-1}$) of $HO_2$ + $C_3F_7CHO$ reaction calculated by the SS-QRRK method.

| $p$ (bar) | 350 $K$ | 330 K | 310 K | 298 K | 290 $K$ |
|---|---|---|---|---|---|
| 0.0316 | 9.86E-16 | 2.34E-15 | 5.55E-15 | 9.30E-15 | 1.31E-14 |
| 0.0667 | 1.95E-15 | 4.49E-15 | 1.02E-14 | 1.65E-14 | 2.26E-14 |
| 0.1 | 2.77E-15 | 6.20E-15 | 1.36E-14 | 2.15E-14 | 2.91E-14 |
| 0.178 | 4.39E-15 | 9.40E-15 | 1.95E-14 | 2.98E-14 | 3.93E-14 |
| 0.316 | 6.60E-15 | 1.34E-14 | 2.62E-14 | 3.86E-14 | 4.98E-14 |
| 0.562 | 9.40E-15 | 1.80E-14 | 3.32E-14 | 4.74E-14 | 5.98E-14 |
| 1 | 1.27E-14 | 2.30E-14 | 4.01E-14 | 5.55E-14 | 6.87E-14 |
| 1.78 | 1.63E-14 | 2.81E-14 | 4.64E-14 | 6.24E-14 | 7.59E-14 |
| 3.16 | 2.01E-14 | 3.28E-14 | 5.17E-14 | 6.78E-14 | 8.14E-14 |
| 5.62 | 2.38E-14 | 3.69E-14 | 5.59E-14 | 7.19E-14 | 8.54E-14 |
| 10 | 2.70E-14 | 4.02E-14 | 5.89E-14 | 7.47E-14 | 8.80E-14 |
| 31.6 | 3.19E-14 | 4.44E-14 | 6.23E-14 | 7.76E-14 | 9.07E-14 |
| 100 | 3.44E-14 | 4.63E-14 | 6.36E-14 | 7.87E-14 | 9.16E-14 |
| 1000 | 3.58E-14 | 4.72E-14 | 6.42E-14 | 7.91E-14 | 9.21E-14 |
| $p$ (bar) | 270$K$ | 250 $K$ | 230 K | 210 K | 190 K |
| 0.0316 | 3.05E-14 | 7.04E-14 | 1.63E-13 | 3.95E-13 | 1.05E-12 |
| 0.0667 | 4.95E-14 | 1.07E-13 | 2.36E-13 | 5.51E-13 | 1.45E-12 |
| 0.1 | 6.12E-14 | 1.28E-13 | 2.73E-13 | 6.27E-13 | 1.64E-12 |
| 0.178 | 7.81E-14 | 1.55E-13 | 3.20E-13 | 7.17E-13 | 1.85E-12 |
| 0.316 | 9.37E-14 | 1.78E-13 | 3.56E-13 | 7.83E-13 | 2.00E-12 |
| 0.562 | 1.07E-13 | 1.97E-13 | 3.82E-13 | 8.28E-13 | 2.11E-12 |
| 1 | 1.18E-13 | 2.10E-13 | 4.00E-13 | 8.57E-13 | 2.17E-12 |
| 1.78 | 1.26E-13 | 2.19E-13 | 4.12E-13 | 8.75E-13 | 2.21E-12 |
| 3.16 | 1.32E-13 | 2.25E-13 | 4.19E-13 | 8.86E-13 | 2.23E-12 |
| 5.62 | 1.35E-13 | 2.29E-13 | 4.23E-13 | 8.93E-13 | 2.24E-12 |
| 10 | 1.38E-13 | 2.31E-13 | 4.26E-13 | 8.96E-13 | 2.25E-12 |
| 31.6 | 1.40E-13 | 2.33E-13 | 4.28E-13 | 8.99E-13 | 2.26E-12 |
| 100 | 1.41E-13 | 2.34E-13 | 4.29E-13 | 9.01E-13 | 2.26E-12 |
| 1000 | 1.41E-13 | 2.34E-13 | 4.29E-13 | 9.01E-13 | 2.26E-12 |

**Table S10**. The transition pressure $p_{1/2}$ (unit: bar) calculated by the SS-QRRK method for $HO_2$ + XCHO (X= $C_2F_5$ and $C_3F_7$) reactions as functions of temperature.

| $p_{1/2}$ | | |
|---|---|---|
| T/K | $C_2F_5CHO + HO_2$ | $C_3F_7CHO + HO_2$ |
| 190 K | 2.60E-05 | 3.80E-02 |
| 210 K | 5.50E-05 | 4.10E-02 |
| 230 K | 1.20E-04 | 5.50E-02 |
| 250 K | 2.00E-04 | 8.00E-02 |
| 270 K | 4.00E-04 | 1.40E-01 |
| 290 K | 8.50E-04 | 2.60E-01 |
| 298 K | 1.20E-03 | 3.39E-01 |
| 310 K | 1.80E-03 | 5.10E-01 |
| 330 K | 3.50E-03 | 1.08E+00 |
| 350 K | 7.40E-03 | 2.30E+00 |

**Table S11**. The conventional transition state theory (TST) rate constants ($cm^3 \cdot molecule^{-1} \cdot s^{-1}$), incorporating Eckart tunneling and multi-structural torsional anharmonicity corrections, for the hydrolysis of XCHO (X = $C_2F_5$ and $C_3F_7$) over the temperature range of 190 to 350 K.

| T/K | $k_1^h$ [a] | $k_2^h$ [a] | $k_3^h$ [a] | $k_{total}^h$ [b] | $k_{F1}^h$ [c] | $k_{F2}^h$ [c] |
|---|---|---|---|---|---|---|
| 190 K | 4.46E-46 | 3.72E-33 | 2.35E-28 | 2.35E-28 | 3.91E-24 | 1.73E-24 |
| 200 K | 3.32E-45 | 1.15E-32 | 6.57E-28 | 6.57E-28 | 8.22E-24 | 3.65E-24 |
| 210 K | 2.10E-44 | 3.49E-32 | 1.67E-27 | 1.67E-27 | 1.61E-23 | 7.19E-24 |
| 220 K | 1.21E-43 | 1.02E-31 | 3.93E-27 | 3.93E-27 | 2.99E-23 | 1.34E-23 |
| 230 K | 6.54E-43 | 2.85E-31 | 8.58E-27 | 8.58E-27 | 5.25E-23 | 2.35E-23 |
| 240 K | 3.19E-42 | 7.57E-31 | 1.76E-26 | 1.76E-26 | 8.83E-23 | 3.97E-23 |
| 250 K | 1.53E-41 | 1.90E-30 | 3.40E-26 | 3.40E-26 | 1.43E-22 | 6.42E-23 |
| 260 K | 7.14E-41 | 4.54E-30 | 6.24E-26 | 6.24E-26 | 2.22E-22 | 1.00E-22 |
| 270 K | 3.28E-40 | 1.03E-29 | 1.10E-25 | 1.10E-25 | 3.36E-22 | 1.52E-22 |
| 280 K | 1.49E-39 | 2.22E-29 | 1.85E-25 | 1.85E-25 | 4.94E-22 | 2.24E-22 |
| 290 K | 6.68E-39 | 4.59E-29 | 3.01E-25 | 3.01E-25 | 7.08E-22 | 3.22E-22 |
| 298 K | 2.17E-38 | 7.95E-29 | 4.35E-25 | 4.35E-25 | 9.32E-22 | 4.24E-22 |
| 300 K | 2.91E-38 | 9.07E-29 | 4.74E-25 | 4.74E-25 | 9.91E-22 | 4.51E-22 |
| 310 K | 1.23E-37 | 1.73E-28 | 7.25E-25 | 7.25E-25 | 1.36E-21 | 6.21E-22 |
| 320 K | 4.94E-37 | 3.17E-28 | 1.08E-24 | 1.08E-24 | 1.83E-21 | 8.38E-22 |
| 330 K | 1.90E-36 | 5.62E-28 | 1.57E-24 | 1.57E-24 | 2.43E-21 | 1.11E-21 |
| 340 K | 6.96E-36 | 9.68E-28 | 2.23E-24 | 2.23E-24 | 3.17E-21 | 1.45E-21 |
| 350 K | 2.42E-35 | 1.62E-27 | 3.11E-24 | 3.11E-24 | 4.07E-21 | 1.87E-21 |

[a] $k_1^h$, $k_2^h$, *and* $k_3^h$ *are* the rate constants of $C_2F_5CHO$ + n $H_2O$ (n =1-3)

[b] $k_{total}^h = k_1^h + k_2^h + k_3^h$

[c] $k_{F1}^h$ *and* $k_{F2}^h$ are the bimolecular rate constants of HCOOH…$H_2O$ + $C_2F_5CHO$ and HCOOH…$H_2O$ + $C_3F_7CHO$

**Table S12**. Cartesian coordinates and vibrational frequencies of all stationary points at the M06-2X/6-MG3S level of theory.

| Species | Frequencies (in $cm^{-1}$) | Cartesian coordinates |
|---|---|---|
| $HO_2$ | 1264.53 1469.45 3703.61 | O 0.05495200 -0.59867100 0.00000000<br>H -0.87923400 -0.86670000 0.00000000<br>O 0.05495200 0.70700900 0.00000000 |
| $C_2F_5CHO$ | 76.14 88.24 159.52 213.5<br>278.25 304.12 355.64 433.71 435.55<br>521.04 599.55 607.61 707.63 799.34<br>994.8 1148.56 1231.05 1252.28<br>1284.39 1300.29 1371.64 1457.72<br>1908.49 3002.58 | C 0.43125700 0.58360400 0.00002500<br>C 1.75383300 -0.19596400 -0.00005100<br>H 2.63897700 0.46334800 -0.00022000<br>C -0.82992200 -0.29162500 -0.00004000<br>O 1.80883500 -1.38357100 0.00000600<br>F -0.85340400 -1.05426900 1.08126100<br>F -1.90693900 0.48232500 -0.00004100<br>F -0.85345800 -1.05429300 -1.08124300<br>F 0.40460900 1.37024200 1.08865300<br>F 0.40467400 1.37034300 -1.08856700 |
| $C_3F_7CHO$ | 28.36 68.51 86.11 151.32<br>197.61 227.76 265.96 273.41 306.92<br>326.25 349.52 390.1 419.98 500.39<br>538.99 589.31 615.37 657.9 764.49<br>811.3 948.82 1030.2 1145.13<br>1205.96 1254.33 1283.32 1299.59<br>1308.01 1358.17 1405.43 1417.35<br>1909.48 3023.08 | C -1.13098500 -0.34184000 0.17164600<br>C -1.76305400 0.78205600 -0.67560000<br>H -1.88170400 0.53528700 -1.74258900<br>C 0.32657400 -0.67287700 -0.20095200<br>O -2.12020100 1.80109700 -0.18186700<br>F 0.35987800 -0.93303800 -1.51856700<br>F 0.71943900 -1.75501600 0.47021700<br>F -1.19561200 -0.04704000 1.46767500<br>F -1.84545800 -1.46123100 -0.06452000<br>C 1.33284800 0.46042700 0.07349000<br>F 2.52154200 0.11377000 -0.38922400<br>F 0.93032900 1.56164800 -0.55515600<br>F 1.42666100 0.70861100 1.36580000 |
| RC1 | 49.89 54.3 69.28 109.2<br>125.33 197.86 218.09 244.66<br>263.15 304.28 339.82 371.12<br>399.76 469.77 478.49 551.58<br>596.28 628.84 733.54 819.58<br>945.53 1110.85 1237.91 276.05<br>1285.99 1312.73 1318.49 384.56<br>1409.83 1531.54 1861.42 3053.17<br>3479.86 | C -0.14323800 -0.32469500 0.03133500<br>C 0.68380700 0.73922500 0.77183100<br>H 0.74259600 0.60652000 1.86111500<br>C -1.62538900 0.08115600 -0.05520600<br>O 1.16031000 1.66604700 0.18171400<br>F -1.75463600 1.18899900 -0.76727100<br>F -2.33961100 -0.87974700 -0.61187400<br>F -2.08532500 0.30669500 1.17416300<br>F 0.31474000 -0.48775200 -1.21229500<br>F -0.08004000 -1.48589400 0.69565200<br>O 3.26807600 0.04465400 -0.45650400<br>H 2.70382300 0.84536800 -0.56285300<br>O 2.64240800 -0.73654000 0.36336500 |
| TS1 | -476.9 54.98 65.92 104.41<br>154.66 216.36 230.3 285.64 301.67<br>363.47 394.28 469.12 540.17 592.3<br>601.07 660.62 704.59 762.52 836.73<br>958.83 1048.21 1051.48 1186.35<br>1235.56 1272.82 1291.68 1311.73<br>1378.3 1396.5 1411.82 1716.68<br>2021.18 3081.16 | C -0.13189300 -0.42508600 -0.05332300<br>C 0.90058100 0.45896100 0.64970200<br>H 0.88793800 0.36529500 1.74056000<br>C -1.54505200 0.18156200 0.00757600<br>O 1.30283000 1.49559000 0.07746500<br>F -1.59135600 1.32009300 -0.66121800<br>F -2.42700400 -0.65923200 -0.50633000<br>F -1.86413600 0.41555700 1.27906600<br>F 0.19277300 -0.59364500 -1.33891000<br>F -0.17991500 -1.62169600 0.55347700<br>O 3.10966200 0.11060500 -0.30498600<br>H 2.46094800 1.02718800 -0.33669900<br>O 2.35451100 -0.66054500 0.35722600 |
| P1 | 37.5 72.25 123.81 158.39<br>222.33 247.08 271.25 318.43 334.87<br>360.98 395.12 427.67 477.58 538.94 | C -0.04953400 -0.46280100 -0.03049400<br>C 1.00863600 0.42558100 0.64027400<br>H 0.77303800 0.54031400 1.69585400 |

| | | |
|---|---|---|
| | 598.69 647.58 689.43 780.5 843.65<br>904.3 1081.48 1185.79 1235.38<br>1245.18 1271.88 1288.6 1305.75<br>1366.51 1380.99 1413.72 1441.4<br>3158.64 3809.53 | C -1.46324000 0.15183400 0.00011500<br>O 1.12904600 1.64187900 0.05294800<br>F -1.54567100 1.19395500 -0.80931200<br>F -2.35275900 -0.75175100 -0.37749100<br>F -1.74922500 0.54284300 1.23935000<br>F 0.27377900 -0.67830100 -1.31496300<br>F -0.10674100 -1.63982400 0.60653900<br>O 2.88602800 -0.15363300 -0.49655400<br>H 1.46577500 1.52267300 -0.84556300<br>O 2.24887200 -0.33236800 0.61775800 |
| RC2 | 25.43 46.54 56.37 78.32<br>104.15 121.74 171.58 205.18<br>220.67 230.21 265.6 279.61 301.15<br>332.39 340.33 367.19 383.65<br>444.16 472.88 520.25 541.43 600.9<br>619.66 676.86 723.75 794.27<br>909.16 1039.23 1177.15 1224.23<br>1258.76 1273.79 1289.31 1309.55<br>1316.26 1346.59 1392.37 1419.94<br>1531.48 1860.61 3056.66 3482.35 | C 0.48558300 -0.10526900 0.16279000<br>C 1.55518200 0.90831900 0.61267400<br>H 1.69361600 0.98716200 1.69960200<br>C -0.89266500 0.58043800 0.07225400<br>O 2.13011400 1.58602900 -0.18963000<br>F -0.87000300 1.44747700 -0.94132800<br>F -1.09399200 1.25352900 1.21842200<br>F 0.80275900 -0.60169800 -1.03515200<br>F 0.41148100 -1.09930100 1.05995300<br>O 3.85362100 -0.50226500 -0.57087800<br>H 3.43056500 0.35229900 -0.81885200<br>O 3.17906200 -0.96664600 0.43072500<br>C -2.09015300 -0.37272700 -0.13226300<br>F -3.17707400 0.34871200 -0.35925100<br>F -1.87239600 -1.16392600 -1.17053600<br>F -2.28680300 -1.11156800 0.94620100 |
| TS2 | -492.2 30.62 58.93 70.08<br>93.71 151.47 188.53 216.58 233.35<br>240.21 289.46 296.46 339.31<br>364.77 382.42 439.81 522.54<br>541.59 591.21 597.46 617.72<br>696.64 705.87 762.53 813.2 941.5<br>970.62 1046.38 1155.87 1189.76<br>1222.46 1259.78 1273.38 1294.05<br>1307.35 1350.06 1375.13 1404.64<br>1417.31 1713.4 2019.49 3085.65 | C 0.49778600 -0.28298400 0.05901600<br>C 1.69431600 0.51040400 0.59582300<br>H 1.74858600 0.54059800 1.68849700<br>C -0.79284800 0.56077800 0.11427500<br>O 2.19525600 1.40553500 -0.11937400<br>F -0.72649700 1.51285000 -0.81540900<br>F -0.86686100 1.13475700 1.32715100<br>F 0.71951500 -0.65101500 -1.20625300<br>F 0.32380000 -1.38165700 0.81448300<br>O 3.75449000 -0.26721000 -0.43363500<br>H 3.24073700 0.72680600 -0.53960800<br>O 2.94895000 -0.83811600 0.35919100<br>C -2.09695800 -0.23825000 -0.10599700<br>F -3.10375700 0.61113900 -0.24047700<br>F -2.00302700 -0.97312200 -1.20347300<br>F -2.34235800 -1.02726000 0.92652900 |
| P2 | 43.32 56.73 66.67 114.66<br>143.67 188.88 214.81 243.64<br>259.83 288.5 295.96 334.17 344.92<br>363.67 382.77 431.92 445.26<br>523.16 545.8 585.36 616.48 683.26<br>699.26 774.18 840.43 874.86<br>994.27 1169.4 1188.18 1222.57<br>1242.71 1262.36 1271.21 1291.92<br>1308.27 1347.66 1362.1 1395.15<br>1404.65 1444.46 3163.97 3810.22 | C 0.54671200 -0.33335900 0.04624700<br>C 1.77587900 0.39689400 0.61100100<br>H 1.62434700 0.61081600 1.66600500<br>C -0.71726200 0.55716700 0.06300300<br>O 2.06059800 1.53871700 -0.06308900<br>F -0.66102700 1.41986900 -0.95271200<br>F -0.75367500 1.23822900 1.21850200<br>F 0.78132000 -0.70646300 -1.22026300<br>F 0.31068500 -1.43184100 0.78106100<br>O 3.46993900 -0.55086100 -0.56724300<br>H 2.32986100 1.31069600 -0.96336800<br>O 2.86695700 -0.56200900 0.57989000<br>C -2.04039900 -0.23361100 -0.05964100<br>F -3.03029500 0.61410000 -0.29102700<br>F -1.96207100 -1.09146900 -1.06614800<br>F -2.29868500 -0.89251800 1.05694600 |

**Table S13**. Cartesian coordinates and vibrational frequencies of all stationary points at the M11-L/maug-cc-pVTZ level.

| Species | Frequencies (in $cm^{-1}$) | Cartesian coordinates |
|---|---|---|
| $HO_2$ | 1218.98 1510.73 3680.97 | O 0.05488400 -0.59524300 0.00000000<br>H -0.87814100 -0.84899900 0.00000000<br>O 0.05488400 0.70136800 0.00000000 |
| $C_2F_5CHO$ | 68.12 78.18 138.45 198.43 264.68 293.18 354.82 434.8 439.28 529.12 608.28 610.83 716.28 805.4 977.52 1137.89 1227.08 1235.05 1293.62 1317.39 1346.75 1448.15 1930.29 2789.36 | C 0.43273500 0.57746400 -0.00000800<br>C 1.75208800 -0.21865100 -0.00002600<br>H 2.63667700 0.47609000 0.00001700<br>C -0.84825000 -0.28231800 0.00002100<br>O 1.83145900 -1.38766400 -0.00007400<br>F -0.88501600 -1.02950500 1.05645900<br>F -1.89312100 0.48763100 0.00006300<br>F -0.88508500 -1.02948100 -1.05642500<br>F 0.42564300 1.35047400 1.06377100<br>F 0.42560300 1.35046400 -1.06379500 |
| $C_3F_7CHO$ | 22.37 63.42 83.34 134.28 182.2 212.62 247.74 256.88 295.61 319.32 348.84 390.54 419.27 504.48 552.74 601.45 623.72 665.64 775.97 809.07 931.67 1020.47 1131.22 1197.62 1251 1282.23 1298.38 1312.93 1352.77 1381.99 1420.42 1924.71 2816.79 | C -1.14626800 -0.33575200 0.17153900<br>C -1.75950600 0.81360000 -0.65733500<br>H -1.92027700 0.54617100 -1.73399400<br>C 0.31659900 -0.67742900 -0.19819900<br>O -2.05714800 1.84001900 -0.17742100<br>F 0.35122700 -0.94427500 -1.48550500<br>F 0.68453200 -1.74343200 0.46162300<br>F -1.22501100 -0.07268300 1.44537000<br>F -1.85639200 -1.41978100 -0.08371100<br>C 1.34301200 0.44816700 0.07475600<br>F 2.50698400 0.08043700 -0.35449600<br>F 0.98548800 1.52453900 -0.56227700<br>F 1.42588700 0.71321300 1.33552900 |
| RC1 | 47.54 50.65 67.84 109.53 121.78 201.82 208.98 247.86 272.52 333.24 358.41 387.43 412.42 477.61 563.82 568.18 606.27 641.73 743.45 820.65 924.83 1090.36 1226.98 1275.23 1285.51 1292.93 1320.01 1366.93 1399.7 1591.05 1842.51 2850.27 3430.32 | C -0.15776700 -0.36300500 -0.01408800<br>C 0.74968200 0.65762600 0.69212800<br>H 0.83747400 0.49119800 1.79327000<br>C -1.62985000 0.11618500 -0.02111000<br>O 1.21337000 1.58631900 0.11761300<br>F -1.74600100 1.20951300 -0.70355700<br>F -2.39916000 -0.78597000 -0.53691800<br>F -2.01410900 0.34461900 1.20164200<br>F 0.22316700 -0.53756400 -1.25284700<br>F -0.11401800 -1.50948900 0.62117800<br>O 3.30618100 0.10220200 -0.35616800<br>H 2.73711200 0.90066400 -0.42994500<br>O 2.61846300 -0.73185700 0.32975500 |
| TS1 | -483.97 49.31 62.99 99.16 149.71 198.88 213.25 277.23 286.68 362.91 389.88 461.7 509.03 559.32 608.15 666.12 712.3 771.99 833.3 949.37 1026.89 1031.29 1137.04 1223.04 1270.2 1293.53 1316.88 1351.03 1382.16 1399.32 1736.26 2075.84 2872.87 | C -0.13261300 -0.43148600 -0.06182000<br>C 0.91571300 0.46228000 0.60859700<br>H 0.89582200 0.37598100 1.71818500<br>C -1.55026400 0.18492300 0.01559000<br>O 1.31717400 1.47539900 0.03621000<br>F -1.60708900 1.29049200 -0.65184200<br>F -2.42404900 -0.64084900 -0.46544300<br>F -1.84959700 0.42937100 1.25835500<br>F 0.16342900 -0.62211100 -1.32322900<br>F -0.17014600 -1.59466000 0.54859800<br>O 3.11479500 0.11431300 -0.27974800<br>H 2.48009300 1.00696600 -0.33088700<br>O 2.34479900 -0.64439100 0.36110600 |
| P1 | 38.72 66.99 103.59 139.46 206.5 228.45 251.56 309.3 339.85 361.1 | C -0.05819200 -0.47060800 -0.03173000<br>C 1.01932100 0.40643600 0.62766000 |

| | | |
|---|---|---|
| | 398.14 433.36 480.49 553.56 608.56 656.79 705.52 790.19 824.93 854.75 1065.34 1192.28 1198.69 1232.44 1267.96 1292.7 1312.42 1345.65 1390.6 1404.61 1448.05 2995.13 3795.46 | H 0.78795100 0.51336200 1.69695200<br>C -1.47011300 0.16654800 -0.00215500<br>O 1.16472000 1.59654600 0.05345700<br>F -1.54643400 1.17937000 -0.80178400<br>F -2.35374500 -0.71070500 -0.36018100<br>F -1.74680600 0.56279600 1.20614900<br>F 0.25746000 -0.70337200 -1.28666000<br>F -0.12608100 -1.61862900 0.60022600<br>O 2.88699700 -0.09701300 -0.48257300<br>H 1.64002800 1.44300700 -0.76794900<br>O 2.23158000 -0.36900500 0.59019100 |
| RC2 | 22.19 44.23 55.25 68.95 102.98 117.93 159.4 202.6 215.92 221.3 254.94 278.51 325.3 337.69 364.05 377.57 394.91 451.49 526.79 555.67 563.91 613.67 629.41 682.51 728.9 800.9 889.24 1018.21 1164.07 1211.74 1255.82 1267.7 1284.92 1293.55 1319.78 1340.72 1368.64 1416.94 1589.11 1842.83 2852.53 3436.42 | C 0.47959900 -0.17836300 0.11121500<br>C 1.59408600 0.77718200 0.58377900<br>H 1.74731900 0.77444700 1.68988400<br>C -0.87589600 0.56830000 0.09280800<br>O 2.15034600 1.50685900 -0.16752200<br>F -0.84583600 1.46427000 -0.85802900<br>F -1.01504600 1.18623000 1.24762100<br>F 0.74375900 -0.61900700 -1.09069500<br>F 0.39834300 -1.19389700 0.93881400<br>O 3.93860900 -0.36965800 -0.48472000<br>H 3.49988400 0.49117600 -0.66653300<br>O 3.18417700 -0.95158000 0.37048500<br>C -2.12919900 -0.32408100 -0.11987600<br>F -3.16441000 0.44114400 -0.27170400<br>F -1.99397500 -1.05709300 -1.17813000<br>F -2.32770200 -1.08929300 0.90358400 |
| TS2 | -482.41 23.73 55.74 62.5 86.22 142.14 172.73 197.79 215.68 223.89 278.85 282.41 336.9 364.73 381.4 430.06 499.86 530.17 559.95 605.97 627.36 706.03 710.41 770.9 812.7 922.9 967.73 1030.7 1113.51 1169.11 1209.95 1253.78 1265.85 1294.44 1316.09 1339.75 1350.09 1382.74 1413.31 1735.24 2078.43 2877.3 | C 0.50076900 -0.29774700 0.04303600<br>C 1.70795200 0.49976200 0.55920000<br>H 1.75220000 0.52876300 1.67046000<br>C -0.78879300 0.55635900 0.11172700<br>O 2.20558300 1.38040300 -0.14190000<br>F -0.72558300 1.49130400 -0.79744300<br>F -0.84629400 1.12395900 1.29776900<br>F 0.70076700 -0.66873400 -1.19626600<br>F 0.34417500 -1.37016700 0.78862500<br>O 3.76805300 -0.25460300 -0.40257600<br>H 3.26282200 0.71187800 -0.51812000<br>O 2.94532300 -0.82216600 0.35940500<br>C -2.11246100 -0.23097200 -0.09572600<br>F -3.08897900 0.61497800 -0.20179800<br>F -2.05855000 -0.94171600 -1.17694900<br>F -2.34903500 -1.00897200 0.91037200 |
| P2 | 40.49 54.13 60.56 100.34 122.43 170.74 200.53 228.37 238.45 268.91 285.49 334.16 348.12 366.04 382.9 435.44 448.1 528.37 559.36 598 626.14 695.45 708.42 783.56 821.78 837.98 963.71 1159.1 1193.57 1197.4 1218.23 1259.39 1264.93 1293.44 1322.04 1335.43 1357.7 1376.29 1415.17 1449.8 2999.62 3796.42 | C -0.54486100 -0.34729400 -0.03838100<br>C -1.78389700 0.37440000 -0.60214000<br>H -1.63010300 0.57118700 -1.67209800<br>C 0.71554600 0.55563300 -0.05354700<br>O -2.08773100 1.49268100 0.04873600<br>F 0.65816400 1.39615600 0.94453600<br>F 0.73936100 1.23538100 -1.17890800<br>F -0.77634900 -0.72117600 1.19933000<br>F -0.31321200 -1.42241600 -0.75843400<br>O -3.49015000 -0.48022500 0.55325100<br>H -2.49975200 1.22037800 0.87374000<br>O -2.84894700 -0.59197700 -0.55609500<br>C 2.05772900 -0.22186300 0.05454600<br>F 3.01583100 0.62373000 0.27096200<br>F 2.01665200 -1.06475300 1.03777100<br>F 2.31259600 -0.86032800 -1.04099600 |

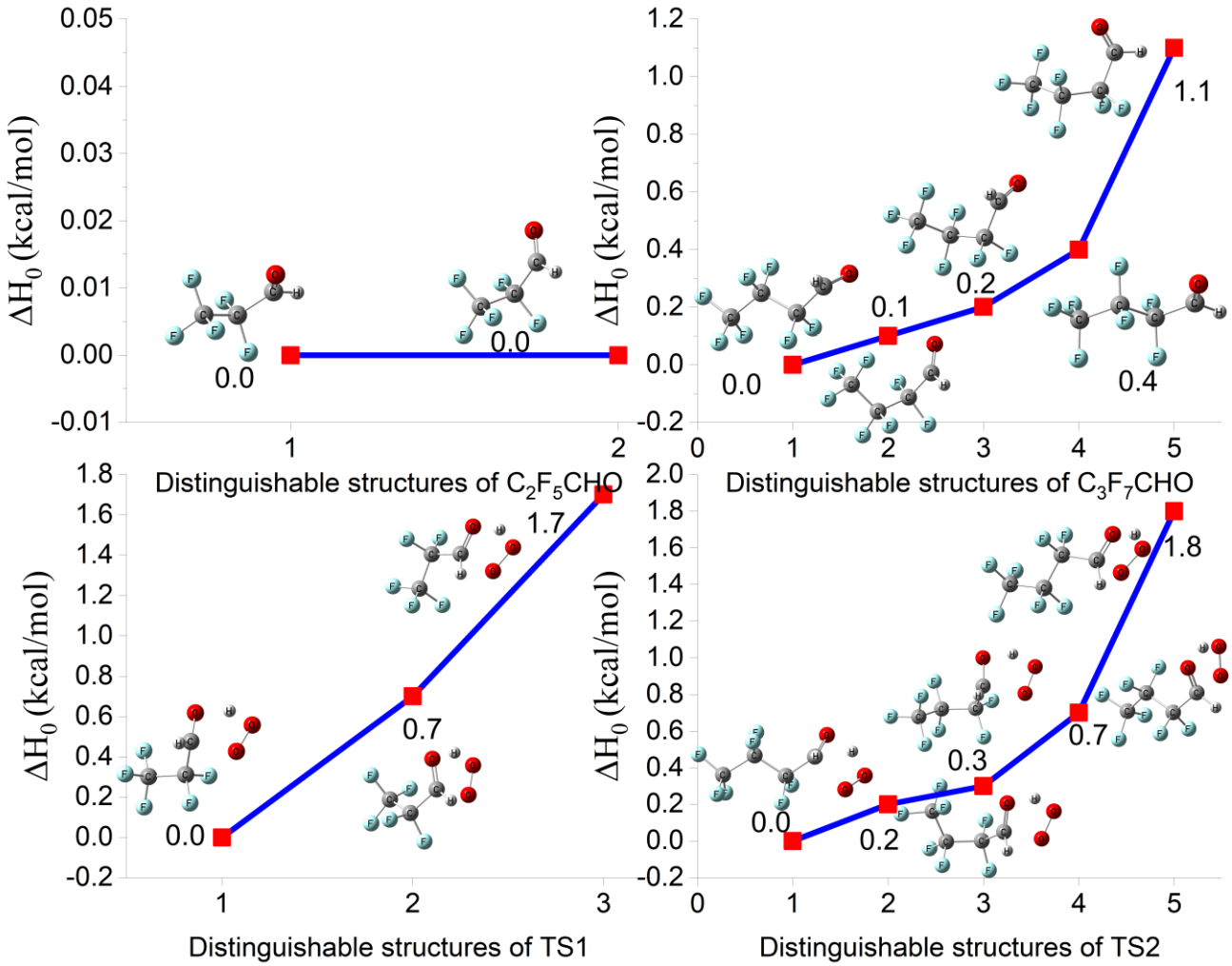


Figure S1. Potential energy distribution of the reactants and saddle point conformations excluding the zero-point energy (ZPE) correction.

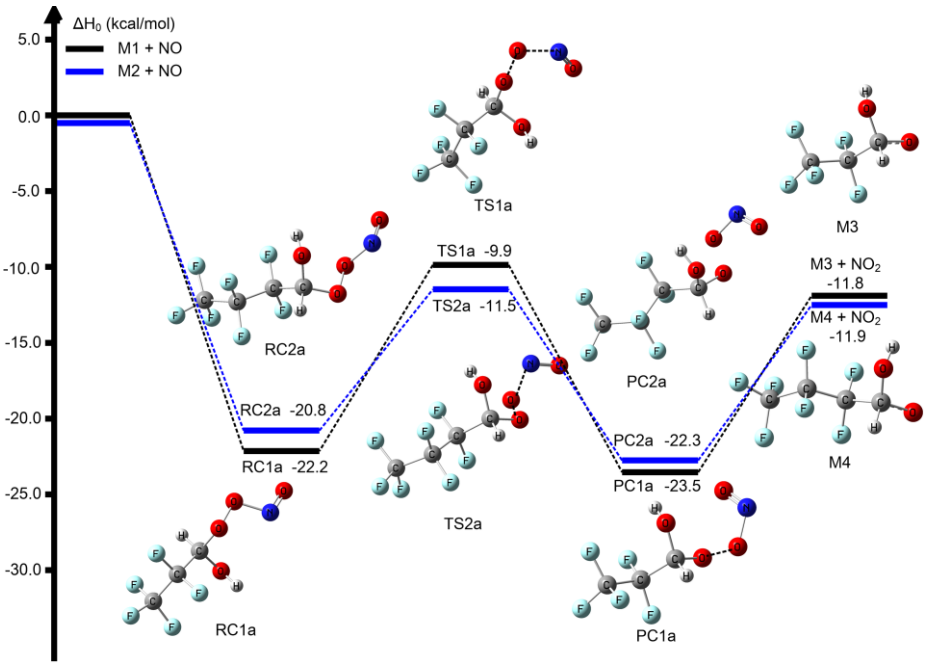


Figure S2. Enthalpy Profile of the Reaction between NO and $C_2F_5CH(OO)OH$ as well as $C_3F_7CH(OO)OH$, calculated at 0 K using the M06-2X/MG3S Method.

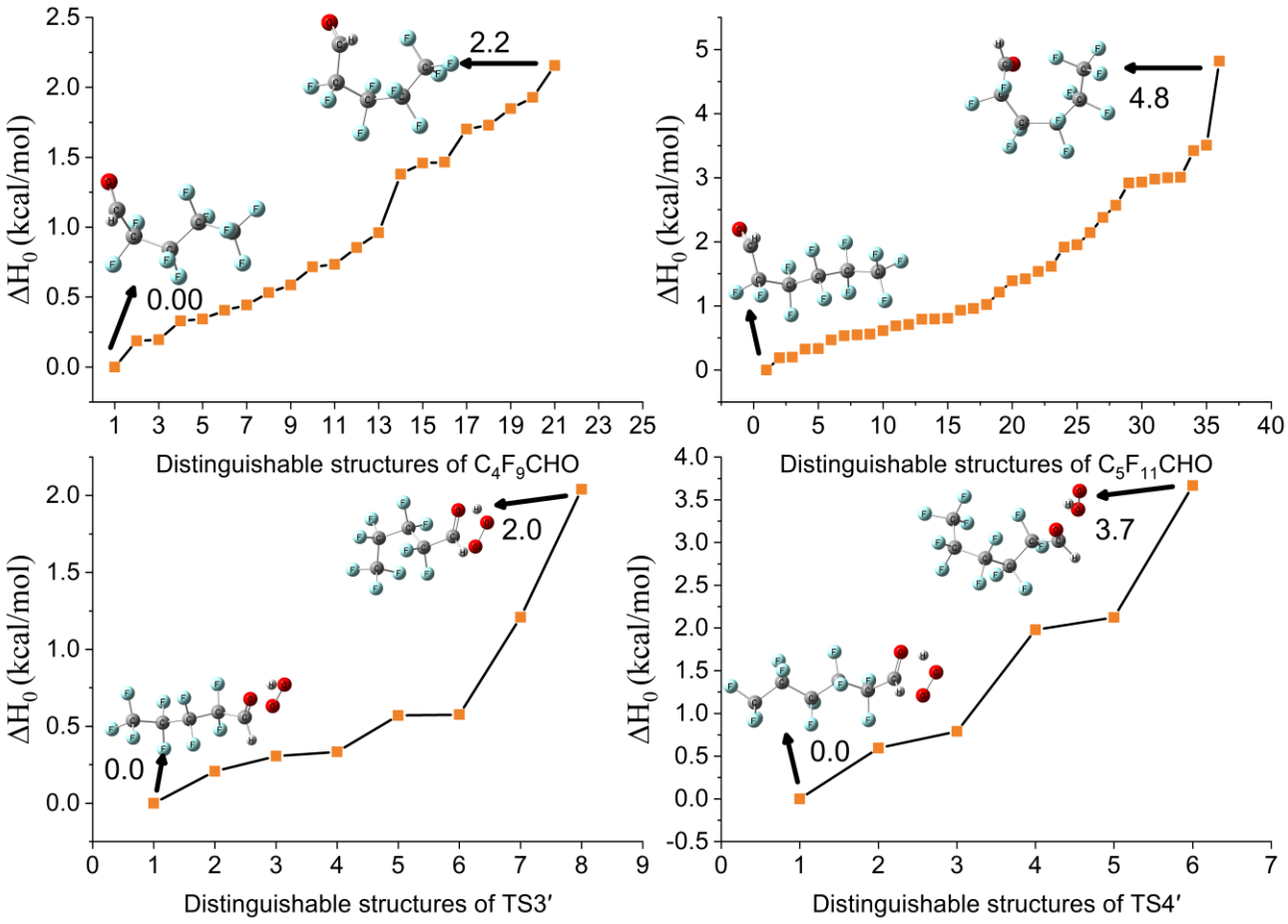


Figure S3. Potential energy distribution of the reactants and saddle point conformations excluding the zero-point energy (ZPE) correction. Geometric optimization was performed at the M06-2X/6-31+G(d,p) level.

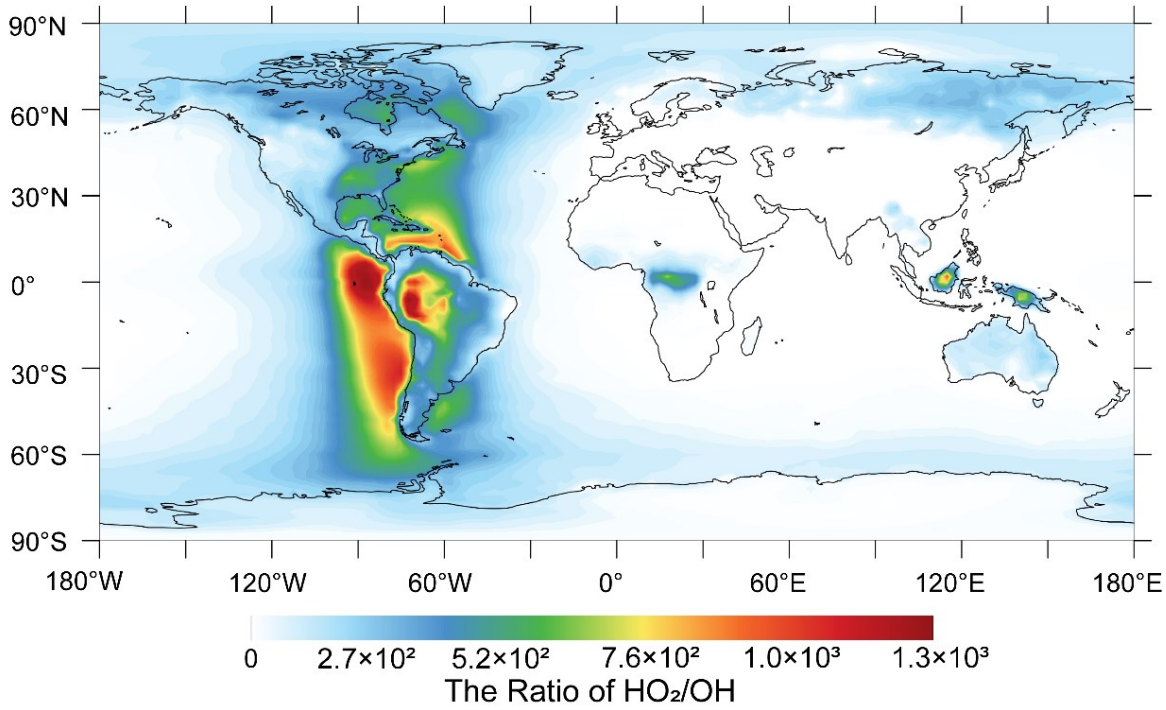


**Figure S4.** The annual average ratio of $HO_2$/OH during the day globally.

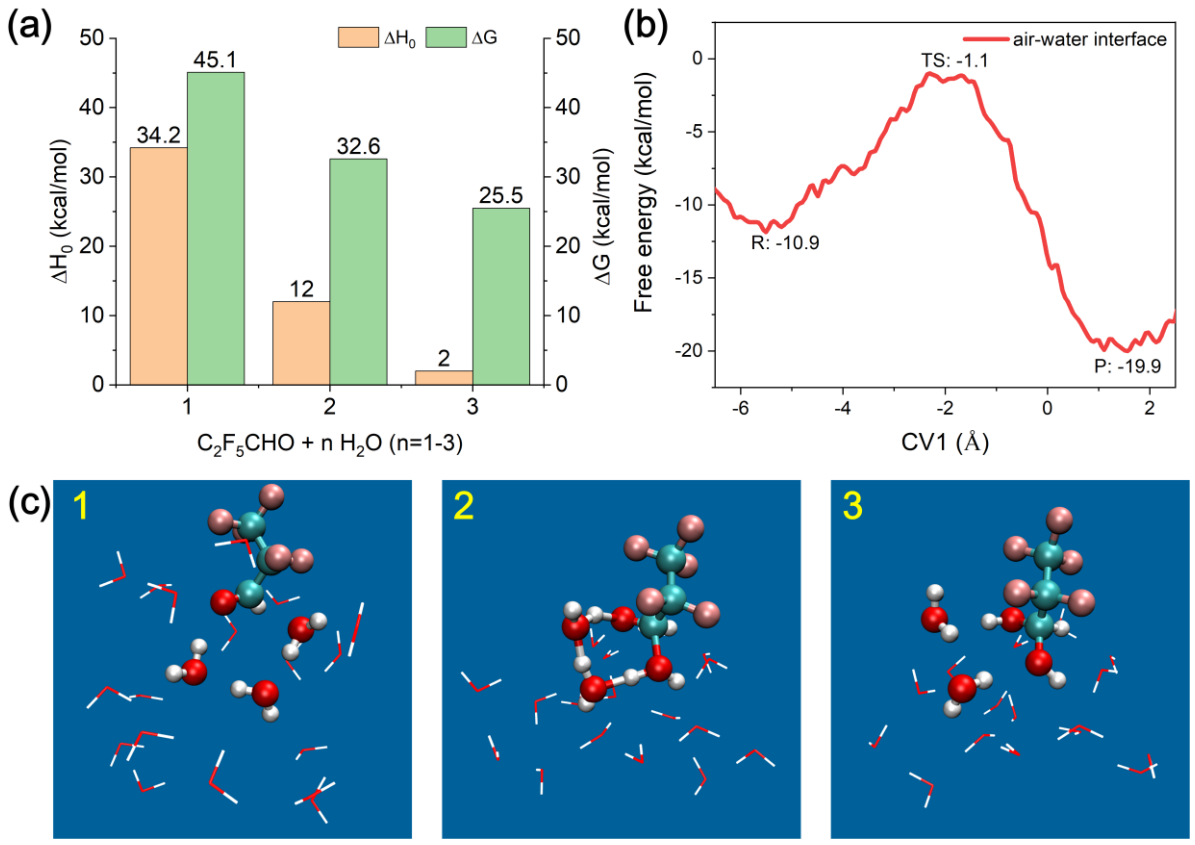


Figure S5. Relative enthalpies ($\Delta H_0$) and Gibbs free energy barriers ($\Delta G$) for the reaction of $C_2F_5CHO$ with n $H_2O$ (n=1-3) (a). Free energy landscape of $C_2F_5CHO$ hydrolysis at the air-water interface(b). Snapshot structures of the reactants, TSs, and products were obtained from the metadynamics-biased AIMD simulations of the $C_2F_5CHO$ hydrolysis reaction (c).

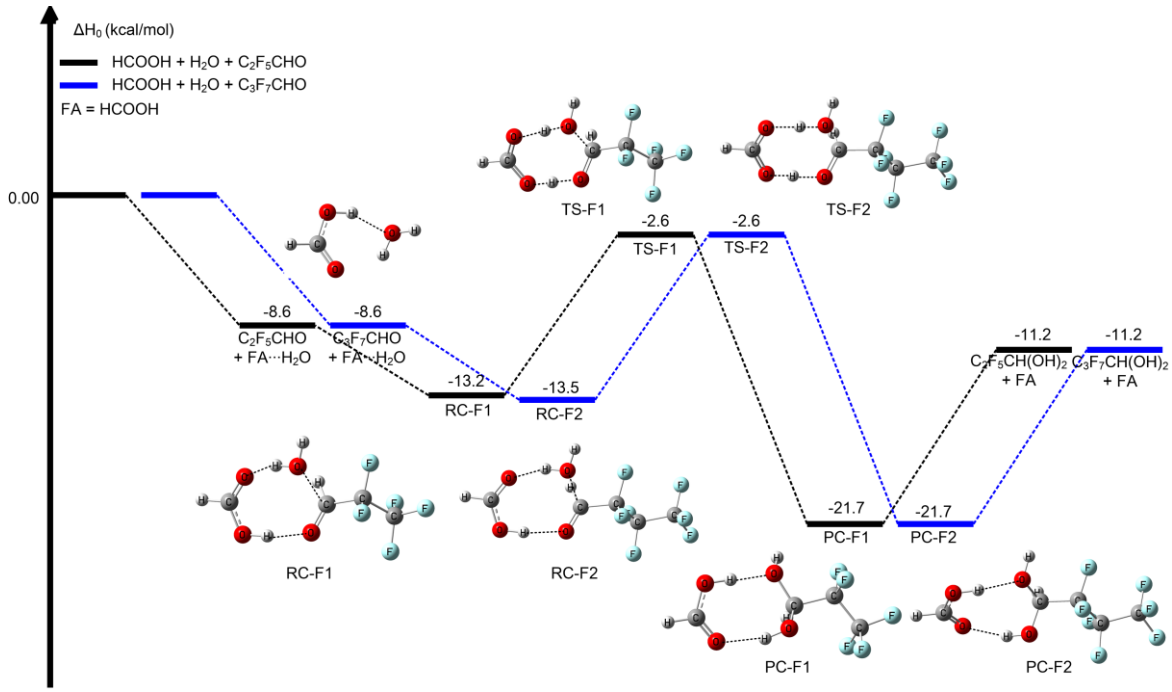


Figure S6. Enthalpy profile for the hydrolysis of $C_2F_5CHO$ and $C_3F_7CHO$ catalyzed by HCOOH, calculated at the FNO-CCSD(T)-F12a/cc-pVDZ-F12//M06-2X/MG3S level at 0 K.

**References**

Bao, J. L. and Truhlar, D. G.: Variational transition state theory: Theoretical framework and recent developments, Chemical Society Reviews, 46, 7548–7596, https://doi.org/10.1039/c7cs00602k, 2017.

Becke, A. D.: Density-functional exchange-energy approximation with correct asymptotic behavior, Physical Review A, 38, 3098–3100, https://doi.org/10.1103/PhysRevA.38.3098, 1988.

Chen, W., Zheng, J., Bao, J. L., Truhlar, D. G., and Xu, X.: MSTor 2023: A new version of the computer code for multistructural torsional anharmonicity, now with automatic torsional identification using redundant internal coordinates, Computer Physics Communications, 288, 108740, https://doi.org/10.1016/j.cpc.2023.108740, 2023.

Fang, Y. G., Li, X., Gao, Y., Cui, Y. H., Francisco, J. S., Zhu, C., and Fang, W. H.: Efficient exploration of complex free energy landscapes by stepwise multi-subphase space metadynamics, Journal of Chemical Physics, 157, 214111, https://doi.org/10.1063/5.0098269, 2022.

Goedecker, S. and Teter, M.: Separable dual-space Gaussian pseudopotentials, Physical Review B - Condensed Matter and Materials Physics, 54, 1703–1710, https://doi.org/10.1103/PhysRevB.54.1703, 1996.

Grimme, S.: Accurate description of van der Waals complexes by density functional theory including empirical corrections, Journal of Computational Chemistry, 25, 1463–1473, https://doi.org/10.1002/jcc.20078, 2004.

Grimme, S.: Semiempirical GGA-type density functional constructed with a long-range dispersion correction, Journal of Computational Chemistry, 27, 1787–1799, https://doi.org/10.1002/jcc.20495, 2006.

Hartwigsen, C., Goedecker, S., and Hutter, J.: Relativistic separable dual-space Gaussian pseudopotentials from H to Rn, Phys. Rev. B, 58, 3641–3662, https://doi.org/10.1103/PhysRevB.58.3641, 1998.

Hoover, W. G. and Alder, B. J.: Studies in molecular dynamics. IV. The pressure, collision rate, and their number dependence for hard disks, The Journal of Chemical Physics, 46, 686–691, https://doi.org/10.1063/1.1840726, 1967.

Kühne, T. D., Iannuzzi, M., Del Ben, M., Rybkin, V. V., Seewald, P., Stein, F., Laino, T., Khaliullin, R. Z., Schütt, O., Schiffmann, F., Golze, D., Wilhelm, J., Chulkov, S., Bani-Hashemian, M. H., Weber, V., Borštnik, U., Taillefumier, M., Jakobovits, A. S., Lazzaro, A., Pabst, H., Müller, T., Schade, R., Guidon, M., Andermatt, S., Holmberg, N., Schenter, G. K., Hehn, A., Bussy, A., Belleflamme, F., Tabacchi, G., Glöß, A., Lass, M., Bethune, I., Mundy, C. J., Plessl, C., Watkins, M., VandeVondele, J., Krack, M., and Hutter, J.: CP2K: An electronic structure and molecular dynamics software package -Quickstep: Efficient and accurate electronic structure calculations, Journal of Chemical Physics, 152, 194103, https://doi.org/10.1063/5.0007045, 2020.

Kuwata, K. T., Hermes, M. R., Carlson, M. J., and Zogg, C. K.: Computational studies of the isomerization and hydration

reactions of acetaldehyde oxide and methyl vinyl carbonyl oxide, Journal of Physical Chemistry A, 114, 9192–9204, https://doi.org/10.1021/jp105358v, 2010.

Laio, A. and Parrinello, M.: Escaping free-energy minima, Proceedings of the National Academy of Sciences of the United States of America, 99, 12562–12566, https://doi.org/10.1073/pnas.202427399, 2002.

Lee, C., Yang, W., and Parr, R. G.: Development of the Colle-Salvetti correlation-energy formula into a functional of the electron density, Physical Review B, 37, 785–789, https://doi.org/10.1103/PhysRevB.37.785, 1988.

Long, B., Xia, Y., and Truhlar, D. G.: Quantitative Kinetics of $HO_2$ Reactions with Aldehydes in the Atmosphere: High-Order Dynamic Correlation, Anharmonicity, and Falloff Effects Are All Important, Journal of the American Chemical Society, 144, 19910–19920, https://doi.org/10.1021/jacs.2c07994, 2022.

Nosé, S.: A unified formulation of the constant temperature molecular dynamics methods, The Journal of Chemical Physics, 81, 511–519, https://doi.org/10.1063/1.447334, 1984.

Troe, J.: Theory of thermal unimolecular reactions at low pressures. II. Strong collision rate constants. Applications, The Journal of Chemical Physics, 66, 4758–4775, https://doi.org/10.1063/1.433838, 1977.

VandeVondele, J. and Hutter, J.: Gaussian basis sets for accurate calculations on molecular systems in gas and condensed phases, Journal of Chemical Physics, 127, 114105, https://doi.org/10.1063/1.2770708, 2007.

Xi, S., Xue, J., Wang, F., and Li, X.: Theoretical study on reactions of α-site hydroxyethyl and hydroxypropyl radicals with $O_2$, Journal of Physical Chemistry A, 125, 5423–5437, https://doi.org/10.1021/acs.jpca.1c00784, 2021.

Zheng, J. and Truhlar, D. G.: Quantum thermochemistry: Multistructural method with torsional anharmonicity based on a coupled torsional potential, Journal of Chemical Theory and Computation, 9, 1356–1367, https://doi.org/10.1021/ct3010722, 2013.